Geophys. J. R. astr. Soc. (1981) **67**, 343–358

A source study of the Thessaloniki (northern Greece) 1978 earthquake sequence

Christos Soufleris *Bullard Laboratories, Department of Earth Sciences, University of Cambridge, Madingley Rise, Madingley Road, Cambridge CB3 0EZ, UK*

Gordon S. Stewart *Seismological Laboratory, California Institute of Technology, Pasadena, California 91125, USA*

Received 1981 January 28; in original form 1980 August 18

Summary. The Thessaloniki (northern Greece) earthquake sequence appears to have occurred along faults forming a graben structure. This graben, situated in the border region between the Serbomacedonian massif and the Vardar zone, is bounded to the south-west by clearly exposed north-west striking north-east dipping normal faults.

Relative hypocentre determinations, fault-plane solutions, surface faulting and the aftershock distribution suggest that some of these faults have been reactivated during the 1978 earthquakes.

The source parameters of the mainshock ($m_b = 6.1$, $M_S = 6.4$) were determined by computing body-wave synthetic seismograms in the time domain and comparing them with the observed. This modelling constrained the orientation of faulting determined by the *P*-wave fault-plane solution. It also constrained the source depth to 6 ± 2 km. Similar depths were calculated by a relative relocation method for the other three large events of the sequence. The dislocation time-function required for the far-field had a total duration of 9 ± 1.5 s, the body-wave moment was $5.2 \pm 1.8 \times 10^{25}$ dyne cm. For a fault length of 35 km and a fault width of 17 km (both estimated from the aftershock distribution) the static stress drop was found to be 4 bar.

An accelerograph record of the mainshock shows two distinct events, 3–4 s apart. These two events were unresolved by the long-period data in the far-field but the unusually long duration of the mainshock time-function suggests an overall slow energy release which probably occurred as a sequence of events close in space and time. Seismic energy released in this fashion can account for waveform complexities observed at some stations.

1 Introduction

In the spring and summer of 1978 a prolonged earthquake sequence occurred in northern Greece. It was centred in an area 25 km east-north-east of the city of Thessaloniki, between the lakes Langadha and Volvi (Fig. 1). It started in early May with several foreshocks (the

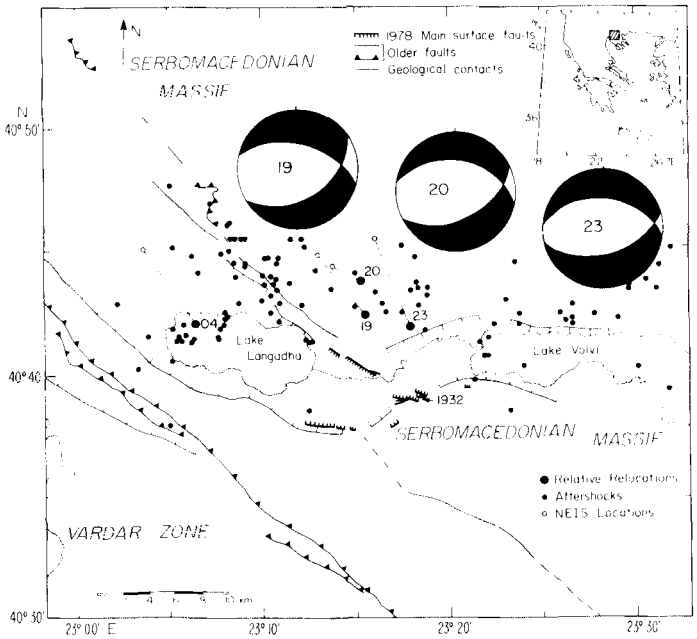

Figure 1. Tectonic setting of the 1978 Thessaloniki earthquake sequence. Faults and major geological contacts are from Kockel & Mollat (1977). Final USGS epicentres are connected to the final relocations of the same events, as determined in this study. Surface ruptures which appeared during the mainshock and are likely to be of tectonic origin are shown with heavy hatched lines on the downthrown side. Preliminary locations for aftershocks, recorded by an array of portable stations, are shown as small solid circles. A fault segment active in 1932 and reactivated in 1978 is marked '1932'.

largest occurring on May 23, $m_b = 5.7$) and culminated on June 20 with a magnitude $m_b = 6.1$, $M_S = 6.4$ mainshock. Considerable aftershock activity followed and lasted for several months (the largest aftershock occurring on July 4, $m_b = 5.1$). Fifty people lost their lives during the mainshock and considerable damage was caused to villages in the epicentral region and to the city of Thessaloniki. The seismic activity was accompanied by surface faulting (Papastamatiou 1978; Mercier *et al.* 1979; Papazachos *et al.* 1979).

The two largest foreshocks and the mainshock were the first major events in that area to have been adequately recorded by WWSSN stations. The present report examines data on the hypocentral locations of the largest earthquakes of the sequence and the source mechanisms of three of these events in an attempt to shed light on the tectonic processes in the region and their relation to the extensional regime of the Aegean (McKenzie 1978).

2 Tectonic setting

The epicentral region consists of a graben structure (the Mygdonian graben), with two lakes occupying its lowest part (Fig. 1). It will be shown subsequently that the largest 1978 earthquakes occurred on west-north-west striking north-north-east dipping normal faults. Faults of similar strike and dip are clearly exposed on the south and south-western edge of the graben. They are part of a major fault system and some of them had been reactivated during the 1978 sequence (Mercier *et al.* 1979; Papazachos *et al.* 1979).

In villages within the epicentral region local inhabitants recollect that in 1932, during a period of high regional seismic activity, normal faulting displacement was observed (north

side downthrown) along a fault segment on the southern part of the graben (see Fig. 1). The same fault segment was reactivated in the same fashion in 1978.

Reactivation of the north-north-east dipping faults has also been documented from the geologic record. Mercier *et al.* (1979) found evidence of dip–slip movements of post-Middle Pleistocene age on faults of similar strike and dip south-west and south-east of Lake Langadha. In the same region they found evidence of dip–slip movements of 'post-Mio–Pliocene, but older than the Recent, age'.

There is also evidence of south dipping normal faults on the northern side of the graben. North of Lake Langadha a clear escarpment is formed on the contact between continental and marine deposits of Miocene-Pliocene age to the north and consolidated alluvial deposits of Pleistocene age to the south. North of Lake Volvi south dipping faults affect the drainage of the valley and the bathymetry of the lake (the lake is deeper on its northern side, Psilovikos 1977). It is not clear when these faults were last active.

In the area shown in Fig. 1 the north-west striking north-east dipping faults form a major fault system which separates the Serbomacedonian massif (a series of Permian and Jurassic carbonates overlying a metamorphic and igneous basement of Upper Carboniferous age) from the Vardar zone (consisting of partly metamorphosed flysch sediments of Upper Jurassic to Lower Cretaceous age). Along some of these faults reverse movements of pre-Tertiary age have been observed (Kockel, Mollat & Walther 1971; Smith & Moores 1974). It therefore appears that extension has reactivated old lines of weakness, resulting in the formation of the graben. It is not clear, however, when the initiation of the graben occurred, but early Neogene time seems possible (Psilovikos 1977).

3 Historical activity

Substantial seismic activity in the area has occurred in historic times in the form of earthquake sequences (Papazachos *et al.* 1979, Fig. 1; Comninakis & Papazachos 1981). In 1759 an earthquake swarm (including a magnitude 6.5 shock near Thessaloniki) lasted for several years and was possibly associated with other large earthquakes further south. In the present century large earthquakes came in two distinct seismic episodes. The first in 1902 ($M \simeq 6.6$) was associated with other events to the north and the south of the region. The sequence lasted for three years. The second in 1932 ($M \simeq 6.9$) was again associated with regional activity which lasted for two years.

4 1978 earthquakes: surface faulting

The 1978 Thessaloniki sequence is one of the few recent (i.e. post-1963) occasions in Greece in which surface faulting was observed following a large shallow earthquake (North 1977; Papazachos *et al.* 1979). In addition its aftershocks have been recorded by a network of locally installed portable stations, operated by a team from the University of Cambridge. Teleseismic hypocentral locations, surface ruptures and locations of the locally recorded aftershocks are being studied to determine the mode of seismic deformation in the region. The present report reviews the surface faulting and deals with teleseismic data. The locally recorded aftershocks are discussed in Soufleris *et al.* (1981).

According to an account of local inhabitants ground cracks appeared at the time of the largest foreshock, on May 23, on the eastern part of the graben. These cracks were not mapped. Reactivation of the existing fault scarps, as well as formation of new ones, occurred during the mainshock on June 20. The surface breaks, interpreted by Mercier *et al.* (1979) as being of tectonic origin, showed normal faulting. These fault breaks are shown in Fig. 1.

However, not all the observed surface breaks were of tectonic origin and some of them had been clearly affected by gravitational sliding in areas of severe topography (Mercier *et al.* 1979). The same authors pointed out that the apparent reverse motion observed on some surface breaks, on sloping ground, was due to normal faulting that became overturned in the unconsolidated sediments at the surface.

A north-west striking 8 km long fault break dips south-west (Fig. 1). It follows the contact between the upper terrace of Pleistocene consolidated material to the north and the lower terrace of Holocene unconsolidated alluvial deposits downthrown to the south. It is the only south dipping main fault scarp activated by the earthquake sequence and it is not clear how it is related to tectonic movements at depth. It may be the surface expression of antithetic faulting at depth, similar to that found by Proffett (1977) in the Basin and Range province of Nevada, USA.

5 Hypocentre locations

Routine teleseismic hypocentral locations for the largest events of the sequence are given by the US Geological Survey (National Earthquake Information Service) and the locations for the four largest events are shown in Fig. 1 and listed in Table 1. The Centre Seismologique Européen Mediterranée (CSEM) epicentre for the mainshock lies within 3 km of the USGS epicentre and at a depth of 15 km. The mainshock has been well recorded teleseismically by stations with good azimuthal distribution and its real location error is not expected to be more than 10–15 km in any direction. Berberian (1979) and Jackson (1980) found location errors of the order of 15 km, for epicentres and depths respectively, for earthquakes of similar magnitude in Iran. For smaller earthquakes, however, poorer azimuthal station coverage combined with systematic and random reading errors and the bias due to the assumed earth model can cause considerably larger location errors, especially in focal depth (Jackson 1980). Departure of the real Earth from the assumed earth model can be responsible for the larger part of these errors.

To improve the teleseismic locations a method of relative relocation (Jackson & Fitch 1979) was employed. The advantage of a relative relocation is that it substantially reduces the bias due to the earth model used. Its basic assumption is that outside the source region ray-paths from nearby events to teleseismic stations are essentially the same. Under this assumption the best recorded event is chosen as the master and all the other events are relocated with respect to it. The mislocation error of the master is largely due to the bias from the assumed earth model and with the relative relocation scheme this bias becomes common to all the relocated earthquakes. Finally, when the absolute position of one or more of these events is accurately known, the pattern can be placed geographically thus removing the earth model bias.

In the present study the mainshock was chosen as the master event and the relocated pattern was placed geographically using the accurate location of the aftershock on July 4 (Carver & Bollinger 1981). This event had been recorded by a network of portable stations and was located below the north-western end of Lake Langadha, at a depth of 8 km. This location agrees with macroseismic data (Comninakis & Papazachos 1979).

Table 1 shows the relocation results and Table 2 shows the determined parameters (i.e. azimuth, polar angle and distance) of each secondary event with respect to the master. To evaluate the quality of the result each location must be viewed together with its corresponding elements in the resolution matrix. The new epicentres (Fig. 1) are in better agreement with the macroseismic data of Comninakis & Papazachos (1979) than the routine teleseismic USGS locations and support macroseismic evidence for a migration of activity towards the

Table 1. USGS locations (†) and final relocation results (*). In the depth column '10G' denotes a fixed depth of 10 km. The standard errors denote internal consistency.

Date	Origin tim.	Lat. (°) N	Lon. (°) E	Depth	m_b
† 1978 May 23	23 34 11.4	40.759	23.268	10G	5.7
* 1978 May 23		40.698 ± 0.009	23.295 ± 0.003	8.5 ± 1.3	
† 1978 June 19	10 31 5.4	40.747	23.216	10G	5.3
* 1978 June 19		40.707 ± 0.015	23.258 ± 0.006	12.0 ± 0.1	
† 1978 June 20	20 3 21.0	40.739	23.229	3.5 ± 4.1	6.1
* 1978 June 20		40.729	23.254	8.0 (Master)	
† 1978 July 4	22 23 28.0	40.751	23.060	18.7 ± 3.9	5.1
* 1978 July 4		40.700 ± 0.007	23.106 ± 0.008	8.0 ± 2.0	

Table 2. Azimuth (Az), polar angle (Pa) and distance (L) for each event with respect to an initial position for the master. This position was the USGS location for that event. The diagonal elements of the resolution matrix are also shown (Jackson & Fitch 1979). Ort is the origin time.

				Resolution matrix				
Date	Az	Pa	L	Rms	Ort	Az	Pa	L
May 23	133.7	89.5	5.1	0.63	0.95	0.88	0.67	0.97
June 19	172.2	35.3	4.4	0.60	0.94	0.74	0.68	0.89
June 20				Master				
July 4	255.1	90.5	12.9	0.61	0.92	0.98	0.90	0.95

north-north-west (also Papastamatiou 1978). A depth of 8–12 km appears to be representative of all four events.

The new locations are accurate to within 3–5 km. This is a consequence of the accuracy within which the teleseismic arrivals are read. This accuracy is within 0.1–1.0 s, depending on the quality of the first arrival and the noise level. Thus changes of the position of the hypocentre of the order of the above reading accuracy times the *P*-wave velocity in the source region (here about 6 km s^{-1}) may not be detectable on the short-period records at teleseismic distances.

Carver & Bollinger (1981) also relocated the same events and their locations are within 2 km to the east or north-east of the locations reported here.

6 Fault-plane solutions

Reliable fault-plane solutions were obtained for the three largest events of the 1978 sequence from long-period data of the WWSSN stations.

All the seismograms were read by the authors. The original records were enlarged 5.5 times and the first-arrival times on the long-period records were compared with those on the short-period records. These time differences were usually within 1 s.

The fault mechanisms for the three largest events are shown in Fig. 2. The epicentral locations of these three events with respect to the surface faulting, the regional tectonic setting and the aftershock distribution suggest that their north dipping plane is the fault plane. There is, however, some uncertainty in the fault plane of the foreshock on June 19. Stations TRI, STU, DBN and KON (see Fig. 2) show a clear compression but their first arrivals on the short-period records are all about 2 s earlier than those on the long-period records. This difference may, for instance, mean that a smaller foreshock occurred before the larger event. However, here it was taken as an indication that these stations lie very close to the node (i.e. the fault plane) and in the dilatational quadrant.

For all three events the inferred fault plane is better constrained than the auxiliary plane.

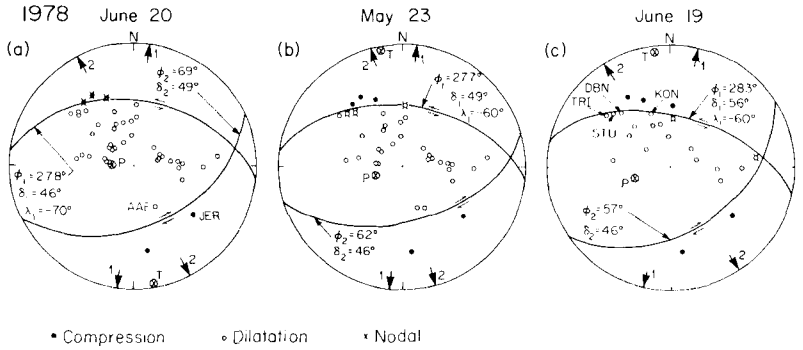

Figure 2. (a, b and c) *P*-wave first-motion data along with the resulting focal mechanisms for the mainshock on June 20 and the two largest foreshocks are shown as equal area projections of their lower focal hemisphere. The horizontal projections of the slip vectors are shown as small arrows. A *P*-wave velocity of 6.8 km s^{-1} at the source was used. ϕ is the strike, δ is the dip of the fault planes and λ the rake (or slip-angle). The rake is measured on the fault plane, from the line of strike (positive anticlockwise).

This causes some uncertainty in the slip-vector direction. However, the slip-vector azimuths of N 332°, N 326° and N 339°, obtained for the two foreshocks and the mainshock respectively, are in close agreement with Mercier *et al.*'s (1979) average slip-vector azimuth of N 333° obtained from measurements on the main surface breaks shown in Fig. 1 (azimuth is measured from north to 360°, positive clockwise). The agreement indicates a close relation between the displacement direction at the surface and that on the earthquake fault at depth.

The fault-plane solutions of Papazachos *et al.* (1979) for the mainshock and the largest foreshock show strike-slip motion with a small reverse component. Their preferred fault plane for the May 23 event has a strike of N 124° and a dip of 78° NE and for the June 20 event (mainshock) a strike of N 124° and a dip of 80° NE. These fault-plane solutions were mainly based on reported polarity readings of both short- and long-period data. More recently Papazachos *et al.* (1981) modified their previous results and their new focal mechanisms for the same events show normal faulting of similar orientation to the one found in the present report. Their new data were mainly from long-period instruments. Their preferred fault plane for the May 23 event had a strike of N 87° and a dip 54° N and for the June 20 event a strike of N 85° and a dip of 36° N. The dip of the fault plane for the latter event is shallower than 46° reported here. They used the same *P*-wave velocity at the source (i.e. 6.8 km s^{-1}) and it appears that their polarity readings differ from ours. However, an aftershock cluster in the hypocentral region of the mainshock defines a plane dipping by about 45° NNE (Soufleris *et al.* 1981); the same dip will be confirmed by the subsequent waveform modelling.

7 Waveform analysis of the mainshock

As a further check on the source mechanisms and depths obtained by conventional methods, WWSSN long-period body-waveforms of the mainshock were analysed. Waveform modelling of the largest foreshock is currently under investigation. These two events were the only earthquakes of the sequence large enough for a meaningful waveform analysis to be carried out.

The waveform analysis was also stimulated by the appearance of an accelerograph record of the mainshock, obtained at a distance of about 25 km from the epicentre. This record exhibits two consecutive groups of *S*-waves suggesting that the earthquake was a double

event (Papazachos *et al.* 1981). The two groups of shear waves arrive with a time difference of 3–4 s, but, because of interference effects, it is difficult to pick the exact *P*-arrival of the second event.

In this study *P*, *SH* and *SV* synthetic waveforms were computed in the time domain and were visually compared with the observed waveforms. The seismographic stations and the types of data used from each station are listed in the appendix. WWSSN stations were selected so that they would provide a good azimuthal coverage and also lie within epicentral ranges of 30° to 90°. In that distance range complications due to upper mantle and core velocity structure are avoided. The long-period vertical components of the *P*-waves and both the horizontal components of the *S*-wave were digitized. The two *S* components were rotated into the back azimuth of the ray to obtain the radial *SV* and tangential *SH* components. Finally the *P*, *SH* and *SV* waveforms were plotted at a uniform time-scale and magnification.

To compute synthetic seismograms, the generalized ray theory for shear dislocations in a layered medium set up by Helmberger (1974) and Langston & Helmberger (1975) was used. Synthetic seismograms were computed by convolving the response of the source region to a shear dislocation with the normalized far-field displacement time history, an attenuation coefficient and the instrument response. The surface interaction at the source region was accounted for. Synthetic and observed waveforms were visually compared and the source model modified until a satisfactory match was achieved.

For the present study the far-field time-function was assumed to be a symmetrical trapezoid, the same for direct and reflected phases, for both the *P*- and *S*-waves. A point-source in a homogeneous half space of *P*-wave velocity 6.0 km s^{-1} and *S*-wave velocity 3.5 km s^{-1} was the initial model. An attenuation coefficient $t^* = 1$ s was assumed for *P*-waves and 4 s for *S*-waves. The direct *P* and the two free surface reflections *pP* and *sP* were considered for the *P* synthetics, *S* and *sS* for the *SH* and *S*, *sS* and *pS* for the *SV*.

At the time of the modelling the Jerusalem (JER) record was not available. The *P*-wave first motion of that station controls the strike of the auxiliary plane in the fault-plane solution (see Fig. 2). The ambiguity was essentially between pure normal faulting, normal with a left-lateral component and normal with a right-lateral component. Thus the first synthetics were computed for stations sufficiently far from the auxiliary plane. These initial runs showed that a source depth of about 6 km and a time function of about 9 s would provide a good match with the observed data. Using these source parameters the *P*-waveform for the station AAE was modelled. This station exhibits a nodal character and a satisfactory match was achieved only with the auxiliary plane passing close to it (see Fig. 6). Thus the normal faulting with a small left-lateral component was established in agreement with the field evidence of Mercier *et al.* (1979) and Papazachos *et al.* (1979).

Fig. 3 shows the *SH*-waveforms at HKC (Hong Kong) and SHL (Shillong). The *SH*-wave radiation pattern of a 45° dip–slip source at teleseismic distances is more sensitive to changes in the source orientation than the *P*-wave radiation. Modelling these two *SH*-waves resulted in a mechanism with left-lateral slip, as was obtained in the *P*-wave modelling, and further constrained the slip-angle. *SH*-waves from these and other stations were more consistent with a strike of N 283° and a dip of 42° N of the fault plane. This is slightly different than N 278° and 46° N obtained from the *P*-wave first motion plot. However, the difference is considered insignificant since there are uncertainties in the *S*-wave radiation pattern and in the positions on the focal sphere of the relatively near stations, which control the strike and dip of the fault plane in the *P*-wave fault-plane solution. *P*-wave synthetics for either mechanism were indistinguishable and the source orientation as deduced from the *P*-wave fault-plane solution was adopted as final. The left-lateral component was later confirmed by the compressional first motion at JER.

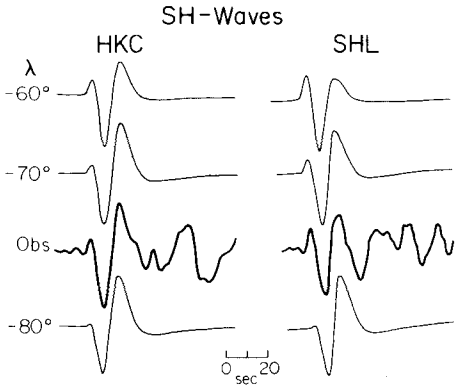

Figure 3. *SH*-wave modelling at WWSSN stations HKC and SHL to constrain the strike of the auxiliary plane of the mainshock, on June 20. Synthetic *SH* seismograms are shown for various rakes. The best fit to the observed data is for $\lambda = -70°$, which corresponds to a strike $\phi_2 = 69°$ and a dip $\delta_2 = 49°$ for the auxiliary, south-east dipping, plane (see Fig. 2). The strike and dip of the fault plane were $\phi_1 = 278°$ and $\delta_1 = 46°$ respectively.

8 Time-function and source depth

By computing synthetics for all the selected stations and for various durations of the time-function and a constant depth of 6 km it was found that a time-function of 9 ± 1.5 s would fit the data satisfactorily. Three of these stations are shown in Fig. 4.

The synthetic waveforms were found to be sensitive to variations of a little less than 2 s in the total duration of the time-function. The first *P*-arrival (first down-swing) of the synthetic waveform was found somewhat sensitive to the duration of the first ramp of the time function. Thus the first down-swing was too impulsive for a ramp of 1 s and too emergent for a ramp of 4 s. A duration of 2 to 3 s of that part of the time-function provided good fits with

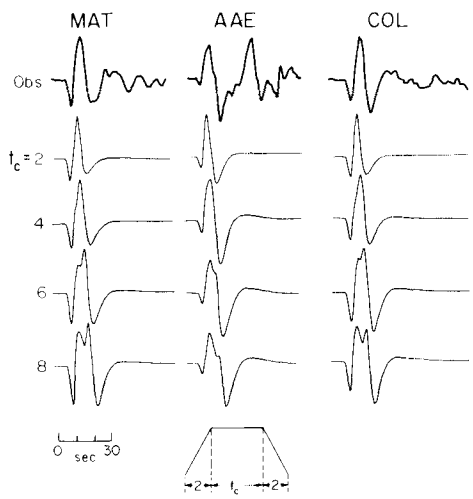

Figure 4. Comparison of observed mainshock *P*-waveforms at MAT, AAE and COL with synthetics for different durations of the time function. The source depth was 6 km. Notice how the width of the first half-cycle, which is sensitive to depth variations (see Fig. 5), remains virtually unaffected by changes in the duration of the time function. The first three half-cycles of the synthetic waveforms from a point source of 9 s (t_c = 4–6 s) duration match the observed satisfactorily.

the observed data. However, the synthetics were insensitive to the duration of the second ramp. It is for this reason that the trapezoid was chosen to be symmetrical and emphasis was placed in resolving its total duration. Similar resolution limits for the different parts of the time-function were found by Cipar (1979) and Ebel (1980).

The duration of the time-function obtained above is unusually long for an earthquake of this size. Similar size earthquakes have been modelled with much shorter time-functions. For example Langston (1976b) modelled the Koyna earthquake ($M_S = 6.4$, $M_0 = 3.2 \times 10^{25}$ dyne cm) with a time-function of 6.5 s, Burdick & Mellman (1976) found a time-function of 5 s for the Borrego mountain earthquake ($m_b = 6.4$, $M_0 = 11.2 \times 10^{25}$ dyne cm). Cipar (1980) modelled the Friuli earthquake ($m_b = 6.1$, $M_S = 6.5$, $M_0 = 1.0 \times 10^{25}$ dyne cm) with a time-function of 4.5 s and Stewart & Helmberger (1981) the Bermuda earthquake ($m_b = M_S = 6.1$, $M_0 = 3.4 \times 10^{25}$ dyne cm) with a time-function of 3 s.

By computing synthetic seismograms for various source depths and a constant time-function of 9 s (Fig. 5) it was found that a depth of 6 ± 2 km would produce synthetics which fit the data satisfactorily. This depth estimate rules out the depth of 15 km calculated by CSEM.

The above calculated depth may be in error due to uncertainties in the *P*- and *S*-wave velocities in the source region. However, the *P*-wave velocity of 6.0 km s^{-1} used here is a good estimate since it results in the minimum rms time residuals when used for the location of the locally recorded aftershocks (Soufleris *et al.* 1981).

Figs 6, 7 and 8 show the observed and synthetic data for the final model.

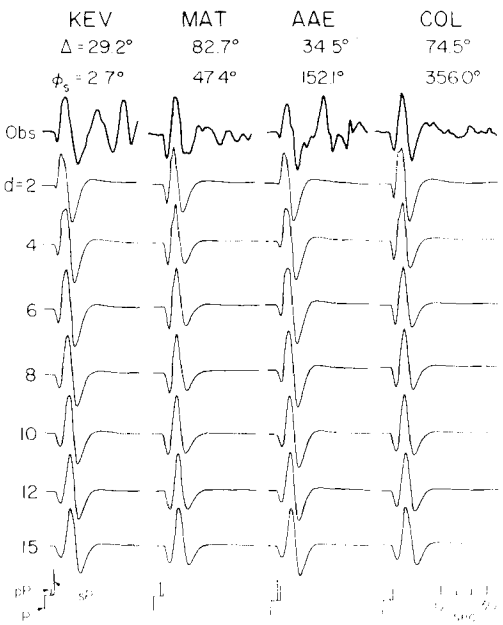

Figure 5. A comparison of observed *P*-waveforms of the mainshock at WWSSN stations KEV, MAT, AAE and COL with synthetic waveforms for various source depths. The relative amplitude of *pP* and *sP* with respect to that of *P* is shown at the bottom of the figure. The duration of the time-function was 9 s. Notice the depth sensitivity of the width of the first pulse, especially at the two nodal stations KEV and AAE. For shallow depths *pP* and *sP* arrive close in time (for a depth of 8 km they arrive with a time difference of 1 s). For the present source orientation they are both compressional (upswing) and their combined amplitude is larger than that of the direct *P*. Therefore they effectively determined the width of the first half-cycle of the waveform, providing a good depth control. The depth which appears most appropriate is 6 km.

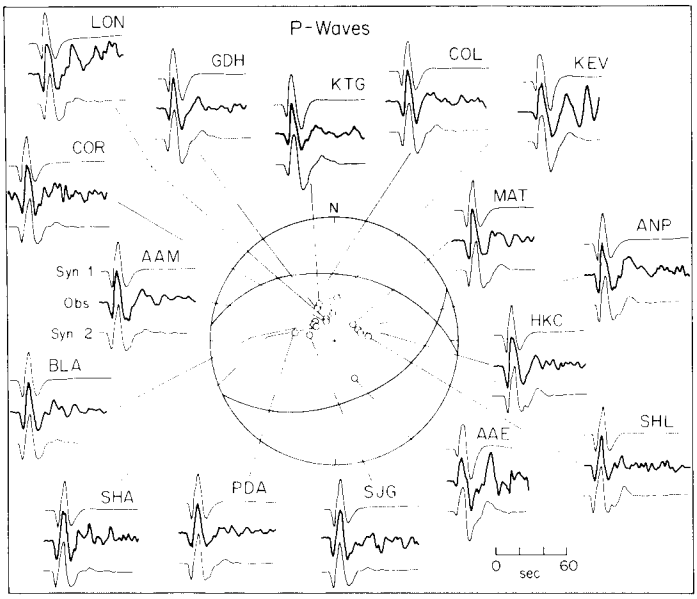

Figure 6. Observed *P*-waves (centre) compared with synthetics from a point source in a homogeneous half space (top) and a layered half space (bottom). The source depth was 6 km and the total duration of the time-function 9 s. Note the similarity of the traces with azimuth around the source, except for the more nodal stations.

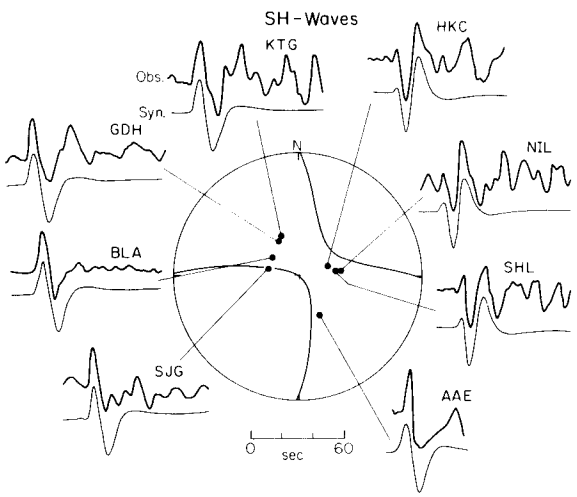

Figure 7. Observed (upper) and synthetics (lower) *SH*-waves as a function of azimuth. The solid curves on the focal mechanism represent nodes in the *SH*-wave radiation. The mechanism and other source parameters are as for Fig. 6.

9 Source in a layered crust – two sources

In the next stage the velocity model in the source region was modified to include the Mohorovičić discontinuity (after Makris 1977) and a low-velocity sedimentary layer (Table 3). *P*-wave synthetics were computed using the Thomson–Haskell layered matrix technique (Haskell 1953, 1962; Langston 1976a). The total source response to a shear dislocation was obtained from a series of matrix multiplications, representing plane waves, at

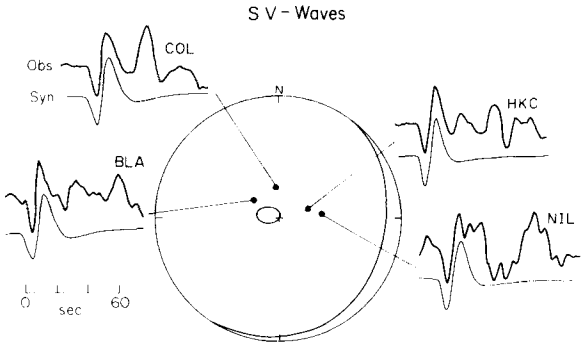

Figure 8. Observed (upper) and synthetic (lower) *SV*-waves as a function of azimuth. The solid curves on the focal mechanism represent nodes in the *SV* radiation. The mechanism and other source parameters are as for Fig. 6.

each frequency. The computation was carried out in the frequency domain and the resulting spectrum was finally transformed into the time domain to obtain the synthetic waveforms (Langston 1976a).

The more elaborate model does seem to produce a somewhat better fit after the third half-cycle (Fig. 6) though it does not explain all the waveform complexities. The close similarity of the *P*-wave synthetics of a point source in a homogeneous half space and a point source in a layered crust for the first 15–20 s suggests that this part of the record is dominated by the *P*, *pP* and *sP* arrivals.

Despite the satisfactory match of the observed data with synthetics from a point source observed (*P*-waveforms at some stations show complexities in the form of phase breaks (see e.g. AAE, KEV, PDA, ANP in Fig. 6). These complexities could be due to lateral heterogeneities in the source region or crustal reverberations at the source or receiver sites. However, the short-period records and the accelerogram show that the earthquake was a multiple event and an attempt was made to model the observed complexities by considering two point sources in a homogeneous half space. Initially there were no means of constraining the second source and it was assumed to have the same mechanism as the first, three times as big a seismic moment (on the short-period records the amplitude of the second event is larger than the amplitude of the first by a factor of about three), the same duration of time-function and to be at the same depth. The two sources were lagged in time by 2–6 s. For time-lags of 2–3 s synthetics from two sources were indistinguishable from those of a single source. For larger time lags the derived synthetics improved the fit at some stations, but they made others worse. The same problem was encountered when we varied the mechanism, depth, moment and time-function of the second source or of both sources. Moreover, because of lack of any constraints for the second source, there was no way of ensuring the uniqueness of the model, considering the complicated tectonics in the source region, and the effort was not pursued further. It appears that the second source is too close to the first in

Table 3. The velocity model used for the computation of synthetic seismograms from a point source in a layered crust.

P-velocity	*S*-velocity	Depth
3.5	2.0	2.0
6.0	3.5	35.0
8.0		

space and in time (about 3 s) and it cannot be distinguished by the long-period instruments in the far-field. Cipar (1979) found that *P*-wave synthetics for the Haicheng earthquake for a single source and for two sources, appropriately scaled and lagged by 3 s, were also indistinguishable in the long-period data at teleseismic distances.

No attempt was made to model the short-period records since any meaningful modelling would require the detailed knowledge of the velocity structure at the source and the receiver sites and these are not known.

The above synthetics were computed for a provisional seismic moment. By comparing the amplitude of the observed and synthetic waveforms the seismic moment of the mainshock was found by calculating the ratio of amplitudes of the first arrivals of each synthetic over the amplitude of the same arrival of the observed. The ratio of amplitudes is equal to the ratio of moments. The average moment calculated from *P*-waves was $5.3 \pm 1.9 \times 10^{25}$ dyne cm from *SH*-waves $5.5 \pm 1.9 \times 10^{25}$ dyne cm and from the *SV*-waves $4.0 \pm 1.1 \times 10^{25}$ dyne cm. The body-wave average was $5.2 \pm 1.8 \times 10^{25}$ dyne cm.

10 Discussion – conclusions

The focal mechanisms of the three largest events of the Thessaloniki sequence show close similarities. The extensional tectonics which prevail in the Aegean and presumably have resulted in the formation of the Mygdonian graben, continue to act at the present time. The motion is taken up by existing faults. The shallow (6–12 km) depths of the largest events of the sequence suggest that seismic deformation in the region is confined to the upper part of the crust.

The pattern of surface faulting which accompanied the earthquake sequence was complicated and it is difficult to establish which fault-breaks are related to the seismogenic fault. Carver & Bollinger (1980, 1981), using the focal mechanisms of Papazachos *et al.* (1979, 1981) and their own joint epicentre locations, preferred the north-west trending south-west dipping fault escarpment as the surface expression of the earthquake fault. This fault scarp, however, dips south-west and our suggestion as representing antithetic movements at depth seems more plausible.

A fault plane with a strike of N 98° and a dip of 45° NNE through the hypocentre of the mainshock intersects the surface at the location of the eastern fault scarp (marked also '1932' in Fig. 1). Further west the same fault intersects the surface half-way between the north dipping and the south dipping fault scarps. It is possible that, as the displacement propagated towards the free surface, it was taken up by movements on different faults.

The main features of the observed body waves for the mainshock were satisfactorily matched with synthetics generated from a point source in a homogeneous half space. From the distribution of aftershocks a fault length of 35 km was taken as a reasonable estimate. Since no aftershock deeper than 12 km was found the width of the 45° dipping fault was taken to be 17 km. Therefore the average displacement along the fault surface, of a static (final) dislocation, was 28 cm. For a dip-slip mechanism the stress drop is given by:

$$\Delta\sigma = [4\mu(\lambda + \mu)/\pi(\lambda + 2\mu)]\, D/w$$

(Kanamori & Anderson 1975). For $\lambda = \mu$, $\Delta\sigma = 2.55\ D/w$ (in bar) and for $D = 28$ cm and $w = 17$ km, $\Delta\sigma = 4$ bar. This low stress-drop value is a consequence of the long duration of the time-function. For constant seismic moment, assuming a constant rupture velocity, high stress-drops are obtained for short durations and low stress-drops for long durations of the time-function (Helmberger & Burdick 1979).

Finally, by assuming that the effective stress σ_e (i.e. initial stress minus the static

frictional stress) is equal to the stress-drop (this effectively means that the final stress along the fault is equal to the static frictional stress, Kanamori & Anderson 1975) and for a shear-wave velocity of 3.5 km s^{-1} and infinite rupture velocity, the dislocation particle velocity is given by: $\dot{D} = 2\sigma_e\beta/\mu$. For $\sigma_e = 4$ bar $\dot{D} = 9$ cm s^{-1}. This is a low value (see, e.g. Brune 1970) and could explain why there was surprisingly little damage in the epicentral area (Papastamatiou 1978; Papazachos *et al.* 1979). However, it must be pointed out that the above low stress-drop is derived for a single source with a long duration of faulting. In reality higher stress-drops and therefore higher dislocation particle velocities and higher accelerations may have occurred locally as sub-sections of the earthquake fault slipped non-uniformly.

An average displacement of no more than 12 cm was observed at the surface along the major fault scarps shown in Fig. 1 (Mercier *et al.* 1979; Papazachos *et al.* 1979). This displacement is 2.5 times smaller than the one calculated above. On the other hand the length of surface faulting is 2 times smaller than the fault length deduced from the aftershocks distribution. It therefore appears that the displacement was reduced as it propagated towards the free surface. It is interesting that the slip-direction along the main fault scarps (Fig. 1), observed at the surface, agrees well with that at depth, but the amount of slip at the surface is smaller than that inferred at depth.

Kulhanek & Meyer (1979) used Brune's (1970, 1971) model and calculated the source parameters for the mainshock from the sum of the spectra of direct and reflected phases of the records at Kiruna and Uppsala. They found a moment of 8.7×10^{25} dyne cm, a fault length of 38.8 km, an average displacement of 24.5 cm and a stress-drop of 5.2 bar. Their results compare favourably with ours despite the fact that they did not correct their spectra for the effect of the free surface (Langston 1978).

The long duration of the mainshock time-function suggests an overall slow energy release, which probably occurred as a sequence of events close in space and time.

Acknowledgments

We greatly benefited from discussions with M. Berberian, J. Cipar, J. Ebel, D. Helmberger, J. Jackson, G. King, D. McKenzie and B. Papazachos. G. Bollinger, J. Dewey, J. Jackson and G. King suggested various improvements to the manuscript.

This research was supported by a grant from the National Academy of Sciences, through WDC-A for seismology, National Science Foundation Grant No. PFR-7921769. CS gratefully acknowledges scholarships from IKY (Greece) and the British Council.

Contribution No. 107, Department of Earth Sciences, University of Cambridge, Cambridge, UK.

Contribution No. 3498, Division of Geological and Planetary Sciences, California Institute of Technology, Pasadena, California 91125, USA.

References

Berberian, M., 1979. Evaluation of the instrumental and relocated epicentres of Iranian earthquakes, *Geophys. J. R. astr. Soc.*, **58**, 625–630.

Brune, J. N., 1970. Tectonic stress and the spectra of seismic shear waves from earthquakes, *J. geophys. Res.* **75**, 4997–5009.

Brune, J. N., 1971. Correction to: 'Tectonic stress and the spectra of seismic waves from earthquakes', *J. geophys. Res.*, **76**, 5002.

Burdick, L. J. & Mellman, G. R., 1976. Inversion of the body waves from the Borrego mountain earthquake to the source mechanism, *Bull. seism. Soc. Am.*, **66**, 1485–1499.

Carver, D. & Bollinger, G. A., 1980. Aftershocks of the June 20, 1978 Greece, earthquake (abstract), *Earthq. Notes*, **50**, 61–62.

Carver, D. & Bollinger, G. A., 1981. Aftershocks of the June 20, 1978 Greece earthquake: a multimode faulting sequence, *Tectonophys.*, in press.

Cipar, J., 1979. Source processes of the Haicheng, China, earthquake from observations of P and S waves, *Bull. seism. Soc. Am.*, **69**, 1903–1916.

Cipar, J., 1980. Teleseismic observations of the 1976 Friuli earthquake sequence, *Bull. seism. Soc. Am.*, **70**, 963–983.

Comninakis, P. E. & Papazachos, B. C. 1979. Distribution of macroseismic effects of the 1978 two major earthquakes in the Thessaloniki area of Northern Greece, *Public. No. 11*, Geophysical Laboratory, Aristoteleian University of Thessaloniki.

Comninakis, P. E. & Papazachos, B. C., 1981. Distribution of the main seismic zone in northern Greece and surrounding area. *Proc. Conf. Intracontinental Earthquakes*, Ohrid, Yugoslavia, in press.

Ebel, J., 1980. Source processes of the 1965 New Hebrides Islands earthquakes inferred from teleseismic waveforms, *Geophys. J. R. astr. Soc.*, **63**, 381–403.

Haskell, N. A., 1953. The dispersion of surface waves on multilayered media, *Bull. seism. Soc. Am.*, **43**, 17–34.

Haskell, N. A., 1962. Crustal reflection of plane P and SV waves, *J. geophys. Res.*, **67**, 4751–4767.

Helmberger, D. V., 1974. Generalised ray theory for shear dislocations, *Bull. seism. Soc. Am.*, **64**, 45–64.

Helmberger, D. V. & Burdick, L. J., 1979. Synthetic seismograms, *Ann. Rev. Earth planet. Sci.*, 7 417–442.

Jackson, J., 1980. Errors in focal depth determination and the depth of seismicity in Iran and Turkey, *Geophys. J. R. astr. Soc.*, **61**, 285–301.

Jackson, J. A. & Fitch, T. J., 1979. Seismotectonic implications of relocated aftershock sequences in Iran and Turkey, *Geophys. J. R. astr. Soc.*, **57**, 209–229.

Kanamori, H. & Anderson, D. L., 1975. Theoretical basis of some empirical relations in seismology, *Bull. seism. Soc. Am.*, **65**, 1073–1095.

Kockel, F., Mollat, H. & Walther, H. W., 1971. Geologie des Serbo–Mazedonischen massivs und seines Mesozoischen Rahmen, *Geol. Jb.*, **89**, 529–551.

Kockel, F. & Mollat, H., 1977. *Geologischen karte der Chelkidhiki und Angrenzender Gebiete, 1: 100,000* (Nord Griechenland).

Kulhanek, O. & Meyer, K., 1979. Source parameters of the Volvi–Langadhas earthquake of June 20 1978 deduced from body-wave spectra at stations UPPSALA and KIRUNA, *Bull. seism. Soc. Am.*, **69**, 1289–1294.

Langston, C. A., 1976a. Body wave synthesis for shallow earthquake sources: inversion for source and earth structure parameters, *PhD thesis*, California Institute of Technology.

Langston, C. A., 1976b. A body wave inversion for the Koyna, India, earthquake of December 10, 1967, and some implications for body wave focal mechanisms, *J. geophys. Res.*, **81**, 2517–2529.

Langston, C. A., 1978. Moments, corner frequencies and the free surface, *J. geophys. Res.*, **83**, 3422–3426.

Langston, C. A. & Helmberger, D. V., 1975. A procedure for modelling shallow dislocation sources, *Geophys. J. R. astr. Soc.*, **42**, 117–130.

McKenzie, D., 1978. Active tectonics of the Alpine Himalayan belt: the Aegean sea and surrounding regions, *Geophys. J. R. astr. Soc.*, **55**, 217–254.

Makris, J., 1977. Geophysical investigations of the Hellenides. Hamburger Geophys, *Einzelschr.*, Reihe A, Heft 34.

Mercier, J. L., Mouyaris, N., Simeakis, C., Roundoyannis, T. & Angelidhis, C., 1979. Intraplate deformation: a quantitative study of the faults activated by the 1978 Thessaloniki earthquakes, *Nature*, **278**, 45–48.

North, R. G., 1977. Seismic moment, source dimensions and stress associated with earthquakes in the Mediterranean and the Middle East, *Geophys. J. R. astr. Soc.*, **48**, 137–161.

Papastamatiou, D. J., 1978. The 1978 Chalkidhiki earthquakes in North Greece: a preliminary field report and discussion, *Technical Note TN LN 28*, Dames & Moore, London.

Papazachos, B. C., Mountrakis, A., Psilovikos, A. & Leventakis, G., 1979. Surface fault traces and fault plane solutions of the May–June 1978 shocks in the Thessaloniki area, North Greece, *Tectonophys.*, **53**, 171–183.

Papazachos, B. C., Mountrakis, A., Psilovikos, A. & Leventakis, G., 1981. Focal properties of the 1978 earthquakes in the Thessaloniki area, *Bulg. Geophys. J.*, in press.

Proffett, J. M., 1977. Cenozoic geology of the Yerington district, Nevada, and implications for the nature and origin of basin and range faulting, *Bull. geol. Soc. Am.*, **88**, 247–266.

Psilovikos, A., 1977. Paleogeographic development of the Mygdonia valley, *PhD thesis*, University of Thessaloniki.

Smith, A. G. & Moores, E. M., 1974. Hellenides, *Mesozoic and Cenozoic Orogenic Belts*, ed. Spencer, A. M., *Spec. Publ. geol. Soc. London*, **4**, 159–185.

Soufleris, C., Jackson, J. A., King, G. C. P., Papazachos, B. C., Scholz, C. H. & Spencer, C. P., 1981. The Thessaloniki (N. Greece) 1978 earthquakes: a delayed multiple event sequence, *Geophys. J. R. astr. Soc.*, submitted.

Stewart, G. S. & Helmberger, D. V., 1981. The Bermuda earthquake of March 24, 1978: a significant oceanic intraplate event, *J. geophys. Res.*, in press.

Appendix

Stations and waves with their polarity readings used for the waveform modelling of the mainshock, where:

Ep. D. is the epicentral distance (in degrees),
Az_{ES} is the azimuth from the epicentre to the station (in degrees),
Az_{SE} is the azimuth from the station to the epicentre (back azimuth, in degrees),
+ denotes compression (first motion up),
– denotes dilatation (first motion down),
n denotes nodal reading,
? denotes questionable reading.

St.	Ep. D.	Az_{ES}	Az_{SE}	Wave type		
AAE	34.5	152.1	338.9	P-	SH+	SV-?
AAM	74.3	312.6		P-		
ANP	80.0	65.6		P-		
ATU	2.7	174.2		P+		
BAG	84.8	73.0	310.8	P-	SH+	
BKS	95.7	333.2		P-		
BLA	75.6	306.8	49.7	P-	SH+	SV-
BOG	92.5	278.2		P-		
CAR	83.3	278.0	49.9	P-	SH+	SV-
COL	74.5	356.0	7.1	P-	SH+	SV-n
COP	16.6	338.3	150.0	P+n	SH+?	
COR	89.9	336.8		P-		
DAL	88.2	313.1		P-		
DAV	94.7	75.6		P-		
DBN	16.8	318.8		P-		
ESK	22.8	319.0	118.9	P-	SH+?	SV-
GDH	48.0	332.2	84.7	P-	SH+	SV-
GSC	95.9	328.1		P-		
HKC	76.6	72.2	308.6	P-	SH+n	SV-
HNR	130.7	63.1		P-		
IST	4.4	83.2		P-n		
JER	13.2	128.7		P+		
KBS	38.6	356.5	166.2	P-	SH+?	SV-
KEV	29.2	2.7	185.9	P-		SV-
KMR	9.8	321.8		P+n		
KON	20.8	340.4		P-		
LON	87.5	336.7		P-		
MAT	82.8	47.3	316.0	P-	SH+?	SV-?
MHI	28.6	86.9	290.0	P-	SH+?	
NIL	40.1	83.6	295.1	P-	SH+n	SV-
NUR	19.9	2.2	183.2	P-n	SH+	SV-
PDA	37.6	281.8	69.8	P-	SH+?	

St.	Ep. D.	Az_{ES}	Az_{SE}	Wave type		
QUE	36.8	92.4		P-		
KTG	37.6	337.0	117.8	P-	SH+	
SHA	84.8	306.3		P-		
SHI	26.3	105.5		P-		
SHL	58.1	82.3	303.5	P-	SH+n	SV-
SJG	77.9	283.5	51.0	P-	SH-n	SV-
SPA	130.5	180.0		P-		
STU	12.8	313.9		P-		
TAB	18.1	90.7		P-		
TOL	20.8	276.7		P-		
TRI	8.5	308.4		P-		
VAL	25.5	307.5	102.8	P-	SH+	SV-
VIE	9.0	329.6		P+n		
VKA	9.0	329.5		P+n		